A local insulin reservoir ensures developmental progression in condition of nutrient shortage in *Drosophila*

Suhrid Ghosh[1,2*], Weihua Leng[1], Michaela Wilsch-Bräuninger[1], Pierre Léopold[3*] and Suzanne Eaton[1,2]

[1]Max Planck Institute of Molecular Cell Biology and Genetics, Pfotenhauerstraße 108
01307 Dresden, Germany

[2]Biotechnologisches Zentrum, Technische Universität Dresden, Tatzberg 47/49, 01307 Dresden, Germany.

[3]Institut Curie, PSL Research University, CNRS UMR3215, INSERM U934, 26 Rue d'Ulm, 75005 Paris, France.

*Authors for correspondence: ghosh@mpi-cbg.de, pierre.leopold@curie.fr

Summary (129 words, max 150)

Insulin/IGF signalling (IIS) controls many aspects of development and physiology. In *Drosophila*, a conserved family of insulin-like peptides (Ilp) is produced by brain neurosecretory cells and exerts systemic functions. Here, we describe the local uptake and storage of Ilps in the Corpora Cardiaca (CC), a group of alpha cell homolog that produces the glucagon-like hormone AKH. Dilp uptake relies on the expression of Impl2, an IGF-BP that accumulates in the CCs. During nutrient shortage, this specific reserve of Ilps is released and activates IIS in a paracrine manner in the prothoracic gland, securing accelerated entry into pupal development through the production of the steroid hormone ecdysone. We therefore uncover a sparing mechanism whereby local Ilp storage and release activates the production of steroids and ensures early developmental progression in adverse food conditions.

Highlights

- Dilps are uptaken by CC cells through the IGF-BP Imp-L2
- the CC-Dilp store is released upon nutrient shortage and activates IIS through CC projections on the PG
- upon nutrient shortage, IIS activation in the PG ensures an accelerated transition from larval feeding stage to metamorphosis.

Keywords

insulin, ecdysone, nutrition, hormone secretion, Drosophila

Introduction

Insulin and insulin-like growth factors (IGFs) are conserved modulators of growth and metabolic homeostasis. They are produced by specific endocrine organs in response to nutrient availability and stimulate peripheral tissues through two main routes. Circulating insulins and IGFs act in an endocrine manner on distant organs through mechanisms of secretion and action that have been extensively studied (Campbell & Newgard, 2021; Petersen & Shulman, 2018; Tokarz, MacDonald, & Klip, 2018). In several instances, insulin/IGFs are also produced and act locally. This is the case for IGF-I produced in peripheral organs like bone chondrocytes, which acts in an autocrine manner (Wang, Bikle, & Chang, 2013). Local insulin/IGF signalling is also key for the development and homeostasis of the central nervous system, which is separated from the systemic circulation by the blood-brain barrier (Fernandez & Torres-Alemán, 2012). In mammalian brains, IGF-I expression is spatially and temporally controlled, participating in the rapid proliferation of neural stem cells (NSCs) (Popken et al., 2004). IGF-I is expressed in neurons, astrocytes and NSCs, contributing to both paracrine and autocrine signaling (D'Ercole & Ye, 2008).

In the *Drosophila* model, a subset of insulin/IGFs called *Drosophila* insulin-like peptides (Dilps) is expressed in neurosecretory cells and contributes to systemic activation of insulin/IGF signaling (IIS). Similar to mammals, local brain expression of Dilps in glial cells also contributes to coupling NSC proliferation with systemic metabolic status (Yuan, Sipe, Suzawa, Bland, Siegrist & Id, 2020; Spéder & Brand, 2018).

In parallel, local activation of IIS can be triggered by alternative routes, providing the possibility to uncouple insulin/IGF signaling from nutrient availability. The role of this uncoupling is exemplified in the case of "brain sparing" a phenomenon observed in many species, including human, whereby moderate nutrient deprivation affects primarily body growth, while brain growth is preserved (Cox & Marton, 2009). The molecular mechanism of brain sparing has been addressed in *Drosophila*. It is associated with the specific activation of neuroblast growth through local production of the ligand Jelly belly (Jeb) and activation of the Anaplastic lymphoma kinase (Alk) receptor upstream of PI-3-kinase, even in the absence of nutrients (Cheng et al., 2011).

Here, we unravel a distinct mechanism locally uncoupling insulin release from the presence of nutrients and leading to the maintenance of IIS activation in a key endocrine organ during development. The initial observation of a pool of Dilps accumulating in an endocrine gland called the corpora cardiaca (CC) (S. K. Kim & Rulifson, 2004), suggested the possibility that these insulins could activate IIS under specific conditions, in a way distinct from their systemic function. Indeed, the CC cells do not produce insulins, but rather a glucagon-like hormone called AKH, whose release is stimulated by nutrient shortage. Our present work unravels some features of the mechanism of uptake of insulins by the CCs. We show that, conversely to systemic insulins, CC insulins are released in response to nutrient deprivation. We further demonstrate that

64 the local release of CC insulins upon starvation maintains high IIS levels in the prothoracic gland (PG), which
65 produces the steroid ecdysone. Finally, we establish that the local activation of IIS in the PG secures a fast
66 transition to pupal development in absence of nutrients.
67 Therefore, our work uncovers a distinct mechanism of organ-sparing, whereby a pre-accumulated store of
68 Dilps is released in adverse food conditions and ensures fast developmental progression through steroid
69 production.
70

71 # Results

72 ## Corpora cardiaca cells take up Dilp2 and 5

73 The Corpora Cardiaca (CC) is part of the ring gland (RG), a composite endocrine organ located in
74 the vicinity of the larval central nervous system (CNS) (Figure 1a). Apart from the CC, two other endocrine
75 tissues - the prothoracic gland (PG), which synthesizes ecdysone, and the corpora allata (CA), which
76 synthesizes the juvenile hormone – together form the PG (Figure 1b). CC cells are neurosecretory in nature
77 and extend processes that terminate in the larval aorta and the PG (Figure 1b). The IPCs, located in the pars
78 intercerebralis of the larval brain, also project to the aorta (Figure 1b). Previous work describes a strong
79 accumulation of anti-Dilp2 immunoreactivity in the corpora cardiaca (CC) (S. K. Kim & Rulifson, 2004), in
80 addition to the one observed in the cell bodies of IPCs (Rulifson, 2002). However, whether CC cells express
81 the Dilp2 gene has not been investigated.
82 In order to clarify the presence and production of Dilp2 in CC cells, we co-labelled the IPC
83 projections by over-expressing a GFP-tagged Synaptotagmin-1 (*SYT1-GFP*) using a *dilp2-gal4* driver
84 (*IPC>SYT1-GFP*, Figure 1c) and anti-Dilp2 immunostaining. We confirmed the presence of IPC processes
85 containing DILP2 and innervating the aorta (Figure 1c). Additionally, Dilp2 could also be detected without
86 GFP colocalization in the CC soma (Figure 1c). Expressing *SYT1-GFP* using a CC-specific GAL4 driver (*akh-*
87 *gal4*), we confirmed that Dilp2 indeed co-localizes with GFP in CC cells and their processes projecting on
88 the PG and the aorta (Figure 1d). CC soma also stain for anti- Dilp5, and both Dilp2 and Dilp5 show high
89 degree of subcellular colocalization (Figure 1e), suggesting that these two Dilps may serve a common
90 function in the CCs. Their presence in the soma of the CC cells could either be due to a transient expression
91 in the CCs or their uptake by the CCs from a pool initially produced by the IPCs. To address this point, we
92 specifically knock-down *DILP2* or *DILP5* expression in the IPCs. This led to their loss in CC cells (Figures 1f-i),
93 indicating that the IPCs are the only source of Dilp production, followed by their specific uptake in the CCs.
94 Of note, the knock-down of Dilp5 expression in the IPCs do not affect the uptake of Dilp2 by the CCs (Figure
95 S1).
96

97 IMPL2 mediates the uptake of Dilp2 and Dilp5 in the Corpora cardiaca

98 In addition to the canonical insulin receptor (dInR), *Drosophila* larvae express another insulin-binding
99 protein called IMPL2. IMPL2 binds circulating Dilp2 and 5, resulting in the downregulation of insulin/IGF-
100 signalling (IIS) in target tissues (Figueroa-Clarevega & Bilder, 2015). Beside tumorous imaginal discs and fat
101 body (Figueroa-Clarevega & Bilder, 2015; Lee et al., 2018), which produce a circulating form of ImpL2, a
102 subset of neurons in the larval brain express the IMPL2 gene (Honegger et al., 2008). Using specific anti-
103 ImpL2 antibodies, we also detected IMPL2 in the CCs (Figure 2a). Similar staining patterns between IMPL2
104 and Dilp2 suggests that they may be partially bound inside the CC. Staining for IMPL2 in Dilp2/Dilp5 double
105 knock-out larvae ruled out a possible staining artefact due to cross-reactivity of the respective antibodies
106 (Figure S2). Additionally, our results show that the presence of IMPL2 in the CC is independent of Dilp2 and
107 5 production (Figure S2).

108 IMPL2 binds to Dilps but, unlike dInR, does not have a trans-membrane domain (Roed et al., 2018). A
109 previous study (Bader et al., 2013) showed that a membrane-associated form of IMPL2 produced in a few
110 brain neurons binds Dilp2 and facilitates its contact with dInR, resulting in activation of intracellular IIS
111 signalling. While dInR is recycled to the membrane after endocytosis, the IMPL2-Dilp2 complex is then
112 degraded (Bader et al., 2013). In order to clarify the mechanism of Dilp uptake by the CCs, we knocked-
113 down dInR and IMPL2 and compared the amount of Dilps present in CC cells. dInR and IMPL2 knock-down
114 were first controlled for their efficacies in the wing disc and CC respectively (Figure S4 and S5a). While
115 silencing *dInR* in CCs had no effect on Dilp2 localization, *ImpL2* knock-down significant reduced Dilp2
116 staining in the CC soma (Figures 2b and 2c). Similar results were obtained for Dilp5 localisation (Figure S3).
117 The knock-down of *dInR* reduces CC cell area and shows a slight increase in mean intensities of Dilp2 (Figures
118 2c) and 5 (Figures S3). Silencing Impl2 in CCs did not affect expression of Impl2 in brain neurons (Figures
119 S5b). We conclude from these experiments that CC cells require IMPL2, but not dInR, to take up Dilps. We
120 next ensured that preventing Dilp uptake in the CC does not affect endogenous glucagon-like AKH
121 production by staining CCs with anti-AKH antibodies (Figures 2d and 2e). Therefore, Impl2 silencing in CC
122 cells is an efficient tool to study the physiological function of the pool of Dilps present in the CCs.

123

124 Corpora cardiaca act as a functional Dilp store

125 Larvae lacking Dilp2 and Dilp5 show reduced growth during larval stages, require extended time to develop
126 and produce smaller adults (Grönke, Clarke, Broughton, Andrews, & Partridge, 2010). To evaluate the
127 contribution of the CC store of Dilp2 and Dilp5 to general IIS, we measured the developmental time, larval
128 growth and adult size of animals devoid of Impl2 in CC cells, therefore lacking Dilp accumulation in CCs. We
129 observed that larvae of the *CC>Impl2-RNAi* genotype show approx. 10 hr advanced pupariation compared

130 to controls (Figure 3a). However, pupal volume, as a measure of total larval growth, adult mass and wing
131 area are not modified (Figure 3b-d). This indicates that animals devoid of a CC-Dilp store experience
132 accelerated growth without changing final size. Measuring larval mass across the L3 stage, we indeed found
133 that removal of CC-Dilps leads to an increase in larval growth rate (Figure 3e). Accelerated growth was
134 previously observed upon general increase in intracellular IIS (Brogiolo et al., 2001) or over-expression of
135 *DILP2* (Géminard, Rulifson, & Léopold, 2009; Ikeya et al., 2002) during larval development. When measuring
136 circulating Dilp2 from *CC>Impl2-RNAi* larvae, we found it doubling compared to controls (Figure 3f). To
137 support this finding, we also found elevated levels of fat body IIS at 104hr AEL compared to control
138 genotypes, measured as the relative distribution of the transcription factor dFOXO between nucleus and
139 cytoplasm (Figure 3g and 3h). Therefore, preventing DILP uptake in the CC increases circulating Dilp2 levels,
140 resulting in accelerated growth.
141
142 CC-Dilps are packaged for co-secretion with AKH
143 Our previous results indicate that approximately equal amounts of Dilp circulate in the hemolymph and are
144 sequestered in the CC cells (Figure 3f). We therefore studied the control of secretion of this major pool of
145 CC-Dilp. Based on colocalization using light microscopy, it was previously proposed that in ImpL2-expressing
146 neurons, ImpL2/Dilp2 complexes are degraded through the late endosomal route (Bader et al., 2013). Given
147 the small size of the CC soma, we used electron microscopy to identify DILP-containing structures inside the
148 CC cells (Figure 4a). Stitching several high-resolution images from a single tissue section shows the overall
149 organization of the CC cytoplasm (Figure 4b). The cytoplasm contains large networks of ER, occasionally
150 interspersed with Golgi complexes, and clusters of dense-core secretory vesicles (DCVs) occupying the
151 perinuclear space (Figure 4b). This architecture is in line with the capacity of CC cells to secrete the
152 glucagon-like hormone AKH, and similar observations have been made in other insects (Willey & Chapman,
153 1960). When probed for Dilp5 using immuno-gold staining, CC cells showed high reactivity in clusters of
154 DCVs compared to rest of the cytoplasm (Figures 4c and 4d). Probing simultaneously for Dilp2 and 5 using
155 gold particles of two different sizes, we observed a co-localization of both Dilps in DCVs, but also in multi-
156 vesicular bodies (MVBs) (Figure 4e). MVBs form in the late endocytic pathway and are responsible for
157 recycling and degradation of endocytic compartments (Cosker & Segal, 2014; Sorkin & Von Zastrow, 2009).
158 Alternatively, they also give rise to secretory granules (Gondré-Lewis, Park, & Loh, 2012). Our results
159 therefore suggest that Dilp2 and 5 are taken up and packaged into secretory DCVs, making the CC cells a
160 potential alternative source of insulin in the *Drosophila* larva.
161 CC cells endogenously produce the glucagon-like peptide hormone AKH and release it under nutrient-
162 limiting conditions (S. K. Kim & Rulifson, 2004). When probing CC cells for AKH and Dilp2 using two

differently-sized gold particles, we found that AKH and Dilp2 co-localize in the same DCVs (Figure 4f). We also noted that AKH seems more abundant than Dilp2 in these DCVs (Figure 4g). Therefore, two functionally antagonistic hormones, AKH and Insulins, are co-packaged in the same secretory structures, raising the intriguing possibility that they are released by CC cells in the same physiological context (i.e. limiting nutrients).

CC-Dilps control the time to pupariation under nutrient limitation.

What could be the physiological role of the pool of CC-insulin? During the late larval period, animals pass through a nutrient restriction checkpoint (NRC), beyond which larvae are committed to pupal development even when fully starved (Pan, Neufeld, Connor, et al., 2019). Early observations (Beadle et. al., 1938) indicate that when starved after the NRC, *Drosophila* larvae pupariate earlier than fed controls, as we observed for *CC>w1118* (Figure 5a,b).

Several lines of evidence suggest that the pool of CC-Dilps induces early pupariation upon starvation post-NRC. First, we noticed that, when comparing fed and starved conditions, the acceleration observed for *CC>w1118* controls is absent in the *CC>ImpL2-RNAi* background (Figure 5c). As described before (see Figure 3a,e), fed *CC>ImpL2-RNAi* larvae pupariate earlier than fed *CC>* controls due to accelerated growth, but in *CC>ImpL2-RNAi* larvae, the difference between fed and starved conditions is abrogated (marked as a grey area in Figures 5b,c). We then confirmed that CC-Dilps are released upon low/no nutrient conditions (Figure 5d-g), reminiscent of what is observed for the control of AKH secretion (J. Kim & Neufeld, 2015). The transition into pupal development requires a surge of ecdysone production and previous work indicate that activation of IIS is required for ecdysone biosynthesis by the PG (Boulan, Martín, & Milán, 2013; Colombani, 2005). Therefore, our observation that CC cells send projections to the PG raises the possibility of a local delivery of Dilps to the PG in response to starvation. To test this idea, we compared the levels of circulating Dilp2 in *CC>* and *CC>ImpL2-RNAi* larvae under different nutritional conditions. In fed conditions, suppressing the CC-Dilp pool leads to an increase in circulating Dilp2 (Figure 5h). However, during starvation post-NRC, no circulating Dilp2 is detected either in *CC>* or *CC>Impl2* conditions (Figure 5i), indicating that the release of the CC pool of Dilp2 does not contribute to increasing systemic Dilp2. In parallel, we measured the nucleus/cytoplasm ratio of dFOXO in fat cells as a marker of peripheral IIS (Figure 5j,k). Again, no difference in adipose IIS was observed between *CC>* and *CC>ImpL2-RNAi* larvae starved after the NRC, indicating that under these conditions, CC-Dilp2 does not contribute to general IIS. In contrast, when conducting a similar analysis of the cells of the prothoracic gland, which synthesizes ecdysone, we observe that starvation after the NRC induces an increase in nuclear localization of dFOXO in the PG of *CC>ImpL2-RNAi* but not of *CC>* control animals (Figure 5l,m). This result indicates that CC-Dilps contribute to maintaining a high level of IIS

196 activation in PG cells in response to post-CW starvation. In line with our finding that *CC>ImpL2-RNAi* larvae
197 pupariate earlier under these conditions, we conclude that the pool of CC-Dilps contributes to a local
198 activation of IIS in PG cells, maintaining their capacity to synthesize ecdysone and allowing a premature
199 transition into pupal development in response to late starvation.
200
201

202 Discussion

203 In this study, we re-evaluate a previous observation whereby glucagon-producing cells take up insulin
204 peptides, and demonstrate the relevance of this phenomenon during *Drosophila* larval development. In the
205 course of early studies on *Drosophila* insulin-producing cells (S. K. Kim & Rulifson, 2004), it was indeed noted
206 that larval CC cells strongly label for Dilp2 peptides. This puzzling observation suggested that the larval CC
207 could serve the role of a so-called "neurohemal" organ, storing Dilps for delivery in the general circulation
208 under specific conditions. However, the mechanistic and functional aspects of this Dilp store were unknown.
209 Our study now sheds new light on the role of CC-Dilps, linking them to another unexplained observation,
210 the starvation-induced, premature transition of *Drosophila* larvae into pupal development (Beadle et. al.,
211 1938) .

212 Accelerating development upon post-critical weight starvation

213 *Drosophila* populations can suffer episodes of nutrient limitation, particularly during the larval period when
214 mobility of individuals is limited, preventing them from exploring alternative food sources. When larvae
215 endure full starvation passed the so-called nutrient restriction checkpoint (NRC), an acceleration of
216 pupariation is observed and animals transit faster to an adult reproductive state, with a trade-off on
217 individual size. This contrasts with the observation that Dilp secretion is inhibited by starvation (Géminard
218 et al., 2009), leading to a reduction of circulating hormone levels. Such reduction should indeed affect the
219 production of ecdysone, which relies on IIS in PG cells (Colombani, 2005). Our present work indicates that
220 upon limiting nutrients, CC cells secrete stored Dilps to the PG in a paracrine fashion (through PG-specific
221 projections) without affecting systemic IIS. The CC-derived Dilps sustain IIS in PG cells, providing the
222 necessary signalling input for ecdysone production and accelerated pupariation. Indeed, IIS activation could
223 prevent starvation-induced autophagy in PG cells, which has been shown to block ecdysone production in
224 condition of a pre-NRC starvation, by shunting cholesterol away from the biosynthetic pathway (Pan,
225 Neufeld, & O'Connor, 2019). Recent evidence suggests that alternative nutrient-independent growth
226 factors such as Jelly-belly (Jeb) can also act on PG cells to stimulate IIS and ecdysone production (Pan &
227 O'Connor, 2020). Jeb and Dilps could constitute separate inputs on ecdysone production, explaining why

228 removal of CC Dilps only affects acceleration upon nutrient restriction but does not delay pupariation.
229 Whether CC-Dilps are uniquely targeted to the PG, and through which mechanism, are still open questions.
230

231 Storing Dilps away from general circulation

232 We find that preventing CC-Dilp storage increases circulating levels by 2-fold. This accelerates animal's
233 growth rate during the late larval stages, when circulating Dilp levels wane (compare Figures 3f and 5h ; also
234 see Okamoto & Nishimura, 2015). We also noted that such accelerated larval growth does not affect adult
235 size due a compensatory advance in pupariation. This result suggests an interdependency relationship
236 between the two Dilp reservoirs, whereby the CC-Dilp store forms from ILP-produced insulins that are
237 derouted from the general circulation in conditions of optimal nutrition. It has been described previously
238 that the IPC project their termini in proximity of the CCs onto the aorta. Whether CC-Dilp accumulates
239 through local delivery of IPC-produced Dilps or by uptake from the general circulation is still unknown.
240 Insulins bind to their cognate receptor InR in target tissues and are then co-endocytosed and later degraded
241 (Sopko & Perrimon, 2013; Sorkin & Von Zastrow, 2009). Our study demonstrates that the uptake of Dilps by
242 CC cells does not rely on InR but rather Imp-L2, an alternative insulin-binding protein previously shown to
243 bind circulating Dilps.-This result contrasts with the previously described case of Imp-L2-producing *Hugin*
244 neurons in the larval CNS, where both InR and Imp-L2 are required for Dilp uptake (Bader et al., 2013). This
245 difference might have important functional consequences. In contrast to endocytosed Dilps/Inr complexes,
246 which are prone to degradation, endocytosed ImpL2/Dilp complexes are routed towards storage in DCV, in
247 the absence of local activation of IIS. Dilps are co-packaged with AKH in DCVs, possibly during the DCV
248 maturation phase. This phase is characterized by cargo exchange between endo-lysosomal compartments
249 and immature vesicles budding off from the trans-Golgi network (Topalidou et al., 2016). Recent studies
250 (Gondré-Lewis et al., 2012; Lund, Lycas, Schack, Andersen, & Gether, 2020) suggest that RAB2 and
251 associated proteins are involved in this exchange. However, we do not know if these components
252 participate in routing DILPs and AKH to DCVs in the CC. Further, Dilps are anterogradely transported along
253 the axonal projections in the PG. This process is similar to the transcytosis of various trophic factors and
254 pathogens observed in mammalian nervous systems (Von Bartheld, 2004). Unlike simultaneous uptake and
255 release previously demonstrated in other neuron types (Hémar, Olivo, Williamson, Saffrich, & Dotti, 1997;
256 Von Bartheld, Wang, & Butowt, 2001; Yamashita, Joshi, Zhang, Zhang, & Kuruvilla, 2017), we show here that
257 Dilp uptake and release are temporally separated during larval development. In all, this sheds light on the
258 unique ability of CC neurosecretory cells to convert an endocrine signal like insulin into a paracrine one.
259

In conclusion, we reveal here a mechanism of organ sparing relying on the storage and release of insulins, allowing the maintenance of IIS activation and ecdysone production in a paracrine organ. The existence of such mechanism opens the intriguing possibility that local pools of insulin/IGF could be used in response to environmental signals to maintain IIS signalling in spared organs in other models.

Acknowledgements

This article is dedicated to the memory of our great colleague and mentor Prof./Dr. Suzanne Eaton. We are grateful to Dr. Natalie Dye for her supervision and leadership. We thank Dr.Jonathan Rodenfels, the Eaton and Leopold lab members for insightful discussions and comments on the manuscript. We would also like to thank the BDSC, Prof. Linda Partridge and Dr. Jason Tennessen for providing us with fly lines, Prof. Marc Tatar and Dr. Stephanie Post for sharing reagents, and Dr. Hugo Stocker for gifting us the Imp-L2 antibody. The scientific illustrations were done by Dr. Bertsy Goic. This work was supported by Deutsche Forschungsgemeinschaft (DFG/FOR2682), Max-Planck-Gesellschaft and Institut Curie, INSERM.

Author contributions

Conceptualization, S.G., S.E., P.L., Methodology, S.G., S.E., P.L., Investigation, S.G., W.L., M.W.-B., Writing and editing, S.G., P.L., Funding Acquisition, S.E.; Supervision, S.E., P.L.

Declaration of interests

The authors declare no competing interests.

References

Bader, R., Sarraf-Zadeh, L., Peters, M., Moderau, N., Stocker, H., Kö hler, K., … Hafen, E. (2013). The IGFBP7 homolog Imp-L2 promotes insulin signaling in distinct neurons of the Drosophila brain. *Journal of Cell Science*, *126*(12), 2571–2576. https://doi.org/10.1242/jcs.120261

Beadle, G. W., Tatum, E. L., & Clancy, C. W. (1938). Food level in relation to rate of development and eye pigmentation in Drosophila melanogaster. *The Biological Bulletin*, *75*(3), 447-462.

Boulan, L., Martín, D., & Milán, M. (2013). Bantam miRNA promotes systemic growth by connecting insulin signaling and ecdysone production. *Current Biology*, *23*(6), 473–478. https://doi.org/10.1016/j.cub.2013.01.072

292 Brogiolo, W., Stocker, H., Ikeya, T., Rintelen, F., Fernandez, R., & Hafen, E. (2001). An evolutionarily
293 conserved function of the drosophila insulin receptor and insulin-like peptides in growth control.
294 *Current Biology*, *11*(4), 213–221. https://doi.org/10.1016/S0960-9822(01)00068-9
295 Campbell, J. E., & Newgard, C. B. (2021). Mechanisms controlling pancreatic islet cell function in insulin
296 secretion. *Nature Reviews Molecular Cell Biology*, *22*(2), 142–158. https://doi.org/10.1038/s41580-
297 020-00317-7
298 Cardona, A., Saalfeld, S., Schindelin, J., Arganda-Carreras, I., Preibisch, S., Longair, M., … Douglas, R. J. (2012).
299 TrakEM2 software for neural circuit reconstruction. *PLoS ONE*, *7*(6).
300 https://doi.org/10.1371/journal.pone.0038011
301 Cheng, L. Y., Bailey, A. P., Leevers, S. J., Ragan, T. J., Driscoll, P. C., & Gould, A. P. (2011). Anaplastic
302 Lymphoma Kinase Spares Organ Growth during Nutrient Restriction in Drosophila. *CELL*, *146*(3), 435–
303 447. https://doi.org/10.1016/j.cell.2011.06.040
304 Colombani, J. (2005). Antagonistic Actions of Ecdysone and Insulins Determine Final Size in Drosophila.
305 *Science*, *310*(5748), 667–670. https://doi.org/10.1126/science.1119432
306 Cosker, K. E., & Segal, R. A. (2014). Neuronal signaling through endocytosis. *Cold Spring Harbor Perspectives*
307 *in Biology*, *6*(2). https://doi.org/10.1101/cshperspect.a020669
308 Cox, P., & Marton, T. (2009). Pathological assessment of intrauterine growth restriction. *Best Practice and*
309 *Research: Clinical Obstetrics and Gynaecology*, *23*(6), 751–764.
310 https://doi.org/10.1016/j.bpobgyn.2009.06.006
311 D'Ercole, A. J., & Ye, P. (2008). Minireview: Expanding the mind: Insulin-like growth factor I and brain
312 development. *Endocrinology*, *149*(12), 5958–5962. https://doi.org/10.1210/en.2008-0920
313 Fernandez, A. M., & Torres-Alemán, I. (2012). The many faces of insulin-like peptide signalling in the brain.
314 *Nature Reviews Neuroscience*, *13*(4), 225–239. https://doi.org/10.1038/nrn3209
315 Figueroa-Clarevega, A., & Bilder, D. (2015). Malignant drosophila tumors interrupt insulin signaling to induce
316 cachexia-like wasting. *Developmental Cell*, *33*(1), 47–56.
317 https://doi.org/10.1016/j.devcel.2015.03.001
318 Géminard, C., Rulifson, E. J., & Léopold, P. (2009). Remote Control of Insulin Secretion by Fat Cells in
319 Drosophila. *Cell Metabolism*, *10*(3), 199–207. https://doi.org/10.1016/j.cmet.2009.08.002
320 Gondré-Lewis, M. C., Park, J. J., & Loh, Y. P. (2012). *Cellular Mechanisms for the Biogenesis and Transport of*
321 *Synaptic and Dense-Core Vesicles*. *International Review of Cell and Molecular Biology* (Vol. 299).
322 Elsevier. https://doi.org/10.1016/B978-0-12-394310-1.00002-3
323 Grönke, S., Clarke, D.-F., Broughton, S. J., Andrews, T. D., & Partridge, L. (2010). Molecular Evolution and
324 Functional Characterization of Drosophila Insulin-Like Peptides. *PLoS Genetics*, *6*(2), 18.

https://doi.org/10.1371/journal.pgen.1000857

Hémar, A., Olivo, J. C., Williamson, E., Saffrich, R., & Dotti, C. G. (1997). Dendroaxonal transcytosis of transferrin in cultured hippocampal and sympathetic neurons. *Journal of Neuroscience*, *17*(23), 9026–9034. https://doi.org/10.1523/jneurosci.17-23-09026.1997

Honegger, B., Galic, M., Köhler, K., Wittwer, F., Brogiolo, W., Hafen, E., & Stocker, H. (2008). Imp-L2, a putative homolog of vertebrate IGF-binding protein 7, counteracts insulin signaling in Drosophila and is essential for starvation resistance. *Journal of Biology*, *7*(3). https://doi.org/10.1186/jbiol72

Id, X. Y., Id, C. W. S., Suzawa, M., Id, M. L. B., & Id, E. S. (2020). Dilp-2 – mediated PI3-kinase activation coordinates reactivation of quiescent neuroblasts with growth of their glial stem cell niche, 1–23. https://doi.org/10.1371/journal.pbio.3000721

Ikeya, T., Galic, M., Belawat, P., Nairz, K., Hafen, E., & Zu, C.-. (2002). Nutrient-Dependent Expression of Insulin-like Peptides from Neuroendocrine Cells in the CNS Contributes to Growth Regulation in Drosophila, *12*(02), 1293–1300.

Isabel, G., Martin, J. R., Chidami, S., Veenstra, J. A., & Rosay, P. (2005). AKH-producing neuroendocrine cell ablation decreases trehalose and induces behavioral changes in Drosophila. *American Journal of Physiology - Regulatory Integrative and Comparative Physiology*, *288*(2 57-2), 531–538. https://doi.org/10.1152/ajpregu.00158.2004

Kim, J., & Neufeld, T. P. (2015). Dietary sugar promotes systemic TOR activation in Drosophila through AKH-dependent selective secretion of Dilp3. *Nat Commun*, *6*, 6846. https://doi.org/10.1038/ncomms7846

Kim, S. K., & Rulifson, E. J. (2004). Conserved mechanisms of glucose sensing and regulation by Drosophila corpora cardiaca cells, *431*(September), 316–320. https://doi.org/10.1038/nature02913.1.

Lee, G. J., Han, G., Yun, H. M., Lim, J. J., Noh, S., Lee, J., & Hyun, S. (2018). Steroid signaling mediates nutritional regulation of juvenile body growth via IGF-binding protein in Drosophila. *Proceedings of the National Academy of Sciences of the United States of America*, *115*(23), 5992–5997. https://doi.org/10.1073/pnas.1718834115

Lund, V. K., Lycas, M. D., Schack, A., Andersen, R. C., & Gether, U. (2020). Rab2 drives axonal transport of dense core vesicles and lysosomal organelles, 1–52.

Okamoto, N., & Nishimura, T. (2015). Signaling from Glia and Cholinergic Neurons Controls Nutrient-Dependent Production of an Insulin-like Peptide for Drosophila Body Growth. *Developmental Cell*, *35*(3), 295–310. https://doi.org/10.1016/j.devcel.2015.10.003

Pan, X., Neufeld, T. P., Connor, M. B. O., Pan, X., Neufeld, T. P., & Connor, M. B. O. (2019). A Tissue- and Temporal-Specific Autophagic Switch A Tissue- and Temporal-Specific Autophagic Switch Controls Drosophila Pre-metamorphic Nutritional Checkpoints. *Current Biology*, 1–12.

https://doi.org/10.1016/j.cub.2019.07.027

Pan, X., & O'Connor, M. B. (2020). Coordination among multiple receptor tyrosine kinase signals controls drosophila developmental timing and body size. *BioRxiv*, 1–43. https://doi.org/10.1101/2020.09.01.278382

Park, S., Alfa, R. W., Topper, S. M., Kim, G. E. S., Kockel, L., & Kim, S. K. (2014). A Genetic Strategy to Measure Circulating Drosophila Insulin Reveals Genes Regulating Insulin Production and Secretion. *PLoS Genetics*, *10*(8). https://doi.org/10.1371/journal.pgen.1004555

Petersen, M. C., & Shulman, G. I. (2018). Mechanisms of insulin action and insulin resistance. *Physiological Reviews*, *98*(4), 2133–2223. https://doi.org/10.1152/physrev.00063.2017

Popken, G. J., Hodge, R. D., Ye, P., Zhang, J., Ng, W., O'Kusky, J. R., & D'Ercole, A. J. (2004). In vivo effects of insulin-like growth factor-I (IGF-I) on prenatal and early postnatal development of the central nervous system. *European Journal of Neuroscience*, *19*(8), 2056–2068. https://doi.org/10.1111/j.0953-816X.2004.03320.x

Roed, N. K., Viola, C. M., Kristensen, O., Schluckebier, G., Norrman, M., Sajid, W., … Brzozowski, A. M. (2018). Structures of insect Imp-L2 suggest an alternative strategy for regulating the bioavailability of insulin-like hormones. *Nature Communications*, *9*(1). https://doi.org/10.1038/s41467-018-06192-3

Rulifson, E. J. (2002). Ablation of Insulin-Producing Neurons in Flies: Growth and Diabetic Phenotypes. *Science*, *296*(5570), 1118–1120. https://doi.org/10.1126/science.1070058

Schindelin, J., Arganda-Carreras, I., Frise, E., Kaynig, V., Longair, M., Pietzsch, T., … Cardona, A. (2012). Fiji: An open-source platform for biological-image analysis. *Nature Methods*, *9*(7), 676–682. https://doi.org/10.1038/nmeth.2019

Sopko, R., & Perrimon, N. (2013). Receptor tyrosine kinases in Drosophila development. *Cold Spring Harbor Perspectives in Biology*, *5*(6), 1–31. https://doi.org/10.1101/cshperspect.a009050

Sorkin, A., & Von Zastrow, M. (2009). Endocytosis and signalling: Intertwining molecular networks. *Nature Reviews Molecular Cell Biology*, *10*(9), 609–622. https://doi.org/10.1038/nrm2748

Spéder, P., & Brand, A. H. (2018). Systemic and local cues drive neural stem cell niche remodelling during neurogenesis in drosophila. *ELife*, *7*, 1–16. https://doi.org/10.7554/eLife.30413

Tokarz, V. L., MacDonald, P. E., & Klip, A. (2018). The cell biology of systemic insulin function. *Journal of Cell Biology*, *217*(7), 2273–2289. https://doi.org/10.1083/jcb.201802095

Topalidou, I., Cattin-Ortolá, J., Pappas, A. L., Cooper, K., Merrihew, G. E., MacCoss, M. J., & Ailion, M. (2016). The EARP Complex and Its Interactor EIPR-1 Are Required for Cargo Sorting to Dense-Core Vesicles. *PLoS Genetics*, *12*(5), 1–29. https://doi.org/10.1371/journal.pgen.1006074

Von Bartheld, C. S. (2004). Axonal Transport and Neuronal Transcytosis of Trophic Factors, Tracers, and

391 Pathogens. *Journal of Neurobiology*, *58*(2), 295–314. https://doi.org/10.1002/neu.10315
392 Von Bartheld, C. S., Wang, X. X., & Butowt, R. (2001). Anterograde axonal transport, transcytosis, and
393 recycling of neurotrophic factors: The concept of trophic currencies in neural networks. *Molecular*
394 *Neurobiology*, *24*(1–3), 1–28. https://doi.org/10.1385/MN:24:1-3:001
395 Wang, Y., Bikle, D. D., & Chang, W. (2013). Autocrine and Paracrine Actions of IGF-I Signaling in Skeletal
396 Development. *Bone Research*, *1*, 249–259. https://doi.org/10.4248/BR201303003
397 Willey, R. B., & Chapman, G. B. (1960). The ultrastructure of certain components of the corpora cardiaca in
398 orthopteroid insects. *Journal of Ultrasructure Research*, *4*(1), 1–14. https://doi.org/10.1016/S0022-
399 5320(60)80002-0
400 Yamashita, N., Joshi, R., Zhang, S., Zhang, Z. Y., & Kuruvilla, R. (2017). Phospho-Regulation of Soma-to-Axon
401 Transcytosis of Neurotrophin Receptors. *Developmental Cell*, *42*(6), 626-639.e5.
402 https://doi.org/10.1016/j.devcel.2017.08.009
403
404
405
406
407
408
409
410
411
412
413
414
415
416
417
418

419 # Figure legends

420 **Figure 1. IPC-derived DILPs 2 and 5 accumulate in the corpora cardiaca.**

421 **(a-b)** Neuroanatomy of the larval central nervous system and ring gland complex showing (**b)**innervation of
422 insulin-producing cells(IPC) and the corpora cardiaca(CC).

423 **(c-d)** Maximum z-volume projection of brain and ring gland complex of larvae expressing Synaptotagmin-1-
424 GFP **(c.i and d.i, green)** specifically in the **(c)** IPC (*dilp2*-gal4) or the **(d)** CC (*akh*-gal4). Tissues are co-stained
425 for DILP2 **(c.ii and d.ii, magenta)**. **Solid arrows** denote aortal projections from **(c)** IPC (**white arrow**) and **(d)**
426 CC (**yellow arrow**). **Open arrows** (yellow) show CC projections to the PG. Merged channels **(c.iii and d.iii)**
427 channel show colocalization. Scale bar = 50um

428 **(e)** Wild-type CC soma stained for neuronal marker HRP (**e.i ; gray**), DILP2 (**e.ii, green**) and DILP5 (**e.iii,**
429 **magenta**). Merged channel (**e.iv**) show DILP2 and DILP5 colocalization. **R** = pixel-based Pearson's correlation
430 coefficient between the same. Scale bar = 10um.

431 **(f,h)** CC soma of IPC-specific(*dilp2*-gal4) **(f)**DILP2 RNAi in Dicer2-expressing background or **(h)**DILP5 RNAi
432 (**h.iv-vi**) together with wild-type controls(**f.i-iii and h.i-iii**). Stained for neuronal marker HRP(**f.i, f.iv, h.i and**
433 **h.iv, gray**) and **(f)**DILP2 (**f.ii and f.v, green**) or **(h)**DILP5 (**h.ii and h.v, green**). Merged channels (f.**iii, f.vi, h.iii**
434 **and h.iv**) for clarity. Scale bar = 10um.

435 **(g, i)** Average fluorescence intensity of **(g)**DILP2 or **(i)**DILP5 normalized to the control mean. Each point
436 represents a single CC soma. n =3-7; **= p<0.01, Student's t-test.

437

438 **Figure 2. IMPL2 in the corpora cardiaca is necessary for DILP uptake.**

439 **(a)** CC soma specifically expressing(*akh*-gal4) Synaptotagmin-1-GFP (**a.i, yellow**); stained for nuclei (**a.i,blue**),
440 IMPL2 (**a.ii, red**) and DILP2 (**a.iii, green**).

441 **(b)** CC-specific(*akh*-gal4) RNAi-mediated knockdown of insulin receptor (**b.iv-vi**), IMPL2 (**b.vii-ix**) and wild-
442 type control (**b.i-iii**). Stained for neuronal marker HRP (**b.i, b.iv, and b.vii, gray**) and DILP2 (**b.ii, b.v and b.viii,**
443 **green**). Merged channels (**b.iii, b.iv and b.ix**) for clarity.

444 **(d)** CC-specific(*akh*-gal4) RNAi-mediated knockdown of IMPL2 (**d.vii-ix**) and wild-type control (**b.i-iii**). Stained
445 for neuronal marker HRP (**b.i, b.iv, and b.vii, gray**) and AKH (**d.ii,and d.iv , blue**).

446 **(c, e)** Average fluorescence intensity of **(c)**DILP2 or **(e)**AKH normalized to the control mean. Each point
447 represents a single CC soma. n =3-5; **= p<0.01, ns = p>0.01; Student's t-test.
448 Scale bar = 10um.

449

450

451 **Figure 3. Corpora cardiaca sequesters circulating DILPs.**

452 **(a)** Percentage pupariated of indicated genotype at various timepoints. AEL= after egg-laying. n=6 for each
453 genotype.
454 **(b)** Pupal volume (n= 24), **(c)** adult weight (n=7, 9) and **(d)** adult wing area (n=55, 20) normalized to control.
455 Each point represents a larva/fly in the case of pupal volume or wing area, and mean of a cohort of 8-15
456 flies in the case weight measurements.
457 **(e)** Larval mass of indicated genotype at specified developmental time (n=8-12). Each point represents mean
458 of cohorts of 13-15 flies.
459 **(f)** DILP2-HA-FLAG concentration in larval hemolymph of indicated genotype using driver line *akh*-gal4,dilp2-
460 HF (n=7,5).
461 **(g)** Fat body of indicated genotype stained for nuclei (**g.i and g.iii, blue**) and mCherry (**g.ii and g.iv, red**).
462 White dashed outlines show the position of some nuclei in the mCherry channel. Scale bar = 50um. **(h)**
463 Boxplots showing ratio of nuclear to cytoplasmic mCherry intensity in fat bodies. Lower ratio indicates
464 higher insulin activity. (n= 10)
465 Bar plots show mean and error bars indicate standard deviation. AEL= after egg-laying. **= $p<0.01$, ns =
466 $p>0.01$, **(b-e)** Student's t-test and **(f,h)** two-tailed Mann-Whitney U test.
467
468 **Figure 4. DILPs and AKH colocalize in corpora cardiaca dense-core vesicles.**
469 **(a)** Schematic representation of experimental approach.
470 Electron micrograph of
471 **(b)** the CC soma (epon-embedded sections). N = nucleus, G = Golgi complex, ER = endoplasmic reticulum,
472 and DCV= dense-core vesicle. Scale bar = 500nm.
473 **(c)** Part of cytoplasm in the CC soma (methylacrylate sections). DILP5 labelled with immunogold particles of
474 5nm diameter. Dashed red line indicates area occupied by DCVs. Scale bar = 500nm **(d)** Quantification of
475 gold particle density (no. of particles/um^2) from DCV area (**dashed red line**) or rest of the cytoplasm (**solid**
476 **black line**) from multiple acquisitions (n=4). Bar plot indicates mean.
477 High-resolution electron micrographs of
478 **(e)** a multi-vesicular body (**MVB, e.i**) and a dense-core vesicle(**DCV, e.ii**) in the CC soma. DILP2 and DILP5 are
479 stained by 10nm (**closed arrow**) and 5nm (**open arrow**) immunogold particles respectively. Scale = 100nm.
480 **(f)** DCV area (**f.i**) stained for DILP2 (**10nm gold particle**) and AKH (**5nm gold particle**). Dashed blue box
481 outlines a single DCV (**f.ii**) magnified on the right, DILP2 **(closed yellow arrow)** and AKH (**open gray arrow**).
482 Scale bar = 100nm.
483 **(g)** Histogram showing immunogold particle size vs. frequency distribution in **(f)**, highlighting relative
484 abundance of DILP2 (**yellow**) and AKH (**gray**).

485
486
487 **Figure 5. Corpora cardiaca DILPs enable starvation-induced accelerated pupariation.**
488 **(a)** Experimental setup for larval starvation
489 **(b-c)** Means of percentage pupariation connected across timepoints for the indicated genotype- starved
490 (**dashed line**) or kept feeding (**solid line**) as shown in **(a).** Fed controls are the same as shown in Figure 3a.
491 n=6 for each curve; p-value from two-way ANOVA with repeated measures and Bonferroni's post t-test for
492 multiple comparisons. Error bars indicate +/- S.D. **= p<0.01 and ns = p>0.01
493 **(d,f)** CC soma of genotype **(d)***akh*>w1118 and **(f)***akh*>KIR2.1 stained for HRP(**d.i,d.iv, f.i and fiv; gray)** and
494 DILP2 **(d.ii, d.v, f.ii and f.v; green)**. KIR2.1 expression inactivates neurons through hyperpolarization. Scale
495 bar = 10um.
496 **(e,g)** Average fluorescence intensity of DILP2 normalized to the mean of fed controls. Each point represents
497 a single CC soma. n =3-5.
498 **(h-i)** DILP2-HA-FLAG concentration in larval hemolymph of indicated genotype using driver line *akh*-
499 gal4,dilp2-HF (n=4-5).
500 **(j)** Fat body of indicated genotype stained for nuclei (**j.i and j.iii; blue**) and mCherry (**j.ii and j.iv; red**). White
501 dashed outlines show the position of some nuclei in the mCherry channel. Scale bar = 50um. **(k)** Boxplots
502 showing ratio of cytoplasmic to nuclear mCherry intensity in fat cells (n=5).
503 **(l)** Prothoracic gland of indicated genotype stained for nuclei (**l.i, l.iii, l.v and l.vii; blue**) and mCherry (**l.ii, l.iv,**
504 **l.vi and l.viii; red**). White dashed outlines show the position of some nuclei in the mCherry channel. Scale
505 bar = 10um. **(k)** Boxplots showing ratio of nuclear to cytoplasmic mCherry intensity in prothoracic gland
506 cells. n=4-8.
507 AEL= after egg-laying. **= p<0.01, ns = p>0.01, **(e-g)** Student's t-test and **(h,i,k,m)** two-tailed Mann-Whitney
508 U test.
509
510
511
512
513
514
515

516 # Materials and methods

517 ## Flies

518 All fly lines/crosses were maintained and grown on standard media containing cornmeal, molasses, agar
519 and yeast extract under a 12hour light/dark cycle at 25˚C (unless explicitly stated otherwise).

520 ## List of fly strains used

Strain	Source	Identifier
w1118	BDSC	#5905
IPC-Gal4 (Dilp2-Gal4)	BDSC	#37516
CC-Gal4 (akh-Gal4)	Tennessen et. al., 2011	NA
dFOXO-mCherry	Kankanj et. al., 2016	NA
gDilp2-HA-FLAG	Park et. al., 2014	NA
UAS-SYT1-GFP	BDSC	#6926
UAS-KIR2.1-GFP	BDSC	#6596
UAS-Dcr2	BDSC	#24651
UAS-DILP2-RNAi	BDSC	#31068
UAS-DILP5-RNAi	BDSC	#31378
UAS-InR-RNAi	BDSC	#31037
UAS-IMPL2RNAi	BDSC	#64936
DILP-2,3,5,7 knock-out	BDSC	#30889
ap-Gal4, tub-Gal80TS	Spannl et. al., 2020	NA

521

522 Fly strains *dilp2-Gal4,>dcr2* , *akh-Gal4,Foxo-mCherry* , *akh-Gal4,gdilp2-HF* and *ap-Gal4,tub-Gal80TS,Foxo-*
523 *mCherry* were generated in this paper by crossing the above lines and are available upon request.

524

525 ## Developmental timing and starvation

526 Fly crosses were fed fresh yeast paste and allowed to lay eggs for 3 hours on apple-juice agar plates.
527 Following egg-laying, the plates were stored at 25˚C. After 18-24 hours of incubation, freshly hatched L1
528 larvae were collected in PBS in intervals of 2 hours. In order to prevent overcrowding, no more than 20-30
529 larvae were transferred into a single food vial using a micropipette and shifted to the incubator at 25˚C with
530 12/12 day-night cycle. At specified time after egg-laying, larvae were carefully washed out of the food using
531 PBS. Subsequently they were quickly transferred to 1% agar vials (same quantity as food). Fed controls were

532 not washed out, and left to feed in their original vials. Both starved and fed control vials were returned to
533 the same incubator.
534 For pupariation timing, number of pupae including white pre-pupae were manually counted at fixed
535 intervals as indicated. Counting was stopped when there was no increase for 3-4 consecutive time points.
536 The same dataset have been used in Figure 3a, and to depict fed controls in Figure 5b,c .
537 For all other starvation experiments, starved and fed control larvae were washed out of the agar/food with
538 PBS, rinsed and used in respective assays.
539
540 Weight measurements
541 Larval weight: At specified developmental stage, larvae were collected from food/agar in PBS, washed 3x
542 times to remove stuck food and cold-anesthetized. Female larvae were selected under the microscope to
543 prevent sex-dependent size variation. Cohorts of 13-15 larvae were blotted on a tissue paper (to ensure no
544 extra liquid) and transferred to a pre-weighed 1.5ml micro-centrifuge tube using forceps. The tube with
545 larvae was then weighed using a fine balance (Sartorius).
546 Adult weight: Virgin females (2 days after eclosion) were anesthetized and collected in pre-weighed 1.5ml
547 micro-centrifuge in cohorts of 10 flies per tube. The tube with adult flies was weighed using a fine balance
548 (Sartorius).
549 Average weight in each case was calculated by dividing the weight difference with the number of larvae/flies
550 in each tube.
551
552 Size determination
553 Adult wing area: Females (1 day after eclosion) were collected and stored in isopropanol. Prior to dissection,
554 flies were transferred to a cavity dissection-glass. Care was taken to keep flies submerged in adequate
555 isopropanol at all times. One wing from each fly was dissected using fine forceps (Dumont, No.5-SA) and
556 transferred to a glass slide along with a small amount of isopropanol (in forceps due to capillary action). It
557 is important to keep wings flat on the slide surface. This can be achieved by repeatedly moistening the wings
558 with isopropanol, using forceps. Once the desired number of wings were obtained, 30ul of Euparal (Roth,
559 cat#7356.1) was pipetted on the slide. Next, a glass coverslip (22mm/22mm/17um) was placed covering
560 the entire area on the slide occupied by wings. To ensure absence of air bubbles and minimum displacement
561 in the wings, it is important to place the coverslip starting from one edge. Following mounting, the slides
562 were left to dry for 2 hours prior to imaging. Single wing images were taken using Zeiss Sv11 dissection
563 scope fitted with a CCD camera (Jenoptik ProgRes C10).

564 **Pupal volume:** Pupae (24-30-hours APF) were collected using a wet brush. Following which, they were
565 washed with PBS to dislodge attached food and glue. Each pupa was then transferred to a single well of a
566 transparent 24-well plate and imaged using Zeiss Sv11 dissection scope fitted with a CCD camera (Jenoptik
567 ProgRes C10). Sex determination was done post-eclosion and only females were taken for analysis.
568
569 Dilp2-HF ELISA
570 Nunc MaxiSorp Flat-Bottom plates (Thermo Fisher Scientific) were coated with anti-FLAG M2 antibody
571 (Sigma, cat#F1804) diluted in BupH Carbonate-Bicarbonate Buffer (Thermo Fisher Scientific, cat#28382)
572 overnight at 4˚C. The plates were washed 2x in wash buffer – PBS + 0.2% Tween20 (Sigma, cat#P7949) and
573 blocked in 2% filter-sterilized BSA in PBS overnight at 4˚C. 1mL of hemolymph was collected by bleeding 5-
574 8 heterozygous gDilp2-HF larvae on a clean cavity slide. The hemolymph was diluted in 55mL PBS and
575 centrifuged at 10,000rpm for 10 minutes to remove hemocytes and debris. 50mL supernatant and 1mL of
576 anti-HA-HRP antibody (Roche, cat#12013819001) solution (1:500) was incubated in the coated wells
577 overnight at 4˚C. 100 ml of 1-Step-Ultra TMB-ELISA Substrate (Thermo Fisher, cat#34028) was pipetted to
578 each well and incubated for 30 minutes in dark at room temperature. Reaction was stopped by adding 100
579 ml of 2M sulfuric acid per well. The samples colorized instantly and the absorbance was measured
580 immediately at 450nm using a plate reader (BMG Labtech). Standard curve was generated by self-generated
581 FLAG(GS)HA peptide. The detailed method is described in Park et al., (2014).
582
583 Immunofluorescence
584 Freshly dissected tissue in PBS was fixed with 4% paraformaldehyde (cat#16005, Aldrich) for 20 minutes.
585 After fixation, tissues were thoroughly washed 3-4 times with PBS. The following protocol was used
586 depending on tissue type.
587 **Brain, ring gland and fat body:** Tissues were permeabilized with PBS containing 0.2%(v/v) Triton X-100(Serva
588 Electrophoresis GmbH, cat#37240.01) for 2 hours at room temperature with shaking. Primary incubation
589 with antibody was done overnight in incubation buffer- PBS with 0.2% Triton X-100 (PBST) and 1mg/ml
590 bovine serum albumin (BSA) (Sigma, cat#A2153). Incubation was followed by 3x15 minute washes with the
591 same incubation buffer without antibodies. Secondary incubation was done with antibody diluted in
592 incubation buffer supplemented with 4%(v/v) normal goat serum (NGS) overnight at 4˚C. Tissues were then
593 washed 4X15 minutes in 0.2%PBST and mounted on glass slides using VectaShield H-1000(cat# H-1000-10)
594 mounting medium.
595 **Wing discs:** Discs were permeabilized with PBS containing 0.05%(v/v) Triton X-100 supplemented with
596 1mg/ml bovine serum albumin (BSA) and 250mM NaCl for 3X10 minutes at room temperature with shaking.

597 Primary incubation with antibody was done overnight in incubation buffer- PBS with 0.05% Triton X-100
598 (PBST) and 1mg/ml bovine serum albumin (BSA). Incubation was followed by 3x15 minute washes with the
599 same incubation buffer without antibodies. Secondary incubation was done with antibody diluted in
600 incubation buffer supplemented with 4%(v/v) normal goat serum (NGS) for 2-3 hours. Wing discs were then
601 washed 3X15 minutes in 0.1%PBST and mounted on glass slides using VectaShield H-1000 mounting
602 medium.
603 All washing and incubation steps were performed on a shaker. Fat bodies from late larval stages disintegrate
604 easily and requires extra care while handling, preferably shaking at a low rpm.
605
606 List of primary antibodies

Antibody	Host species	Dilution	Source
Dilp2	Rat	1:400	(Géminard et al., 2009)
Dilp5	Rat	1:1000	This paper
Dilp5	Rabbit	1:500	(Géminard et al., 2009)
Akh	Rabbit	1:800	(Isabel,Martin,Chidami, Veenstra,&Rosay, 2005)
mCherry	Rabbit	1:500	Invitrogen #PA5-34974
GFP	Rabbit	1:500	Invitrogen #A111022
IMPL2	Rabbit	1:1000	(Bader et al., 2013)

607
608 Secondary antibodies/dyes used were DAPI (1:2000 from 5mg/ml stock, Roche), DyLight 405 goat anti-HRP
609 (1:500, Jackson IR, cat#123-475-021), AlexaFlour-488 goat anti-rabbit (1:1000, Invitrogen #A11034),
610 AlexaFlour-568 goat anti-rabbit (1:500, Invitrogen #A11036) and AlexaFlour-647 goat anti-rat (1:500,
611 Invitrogen #A21247).
612
613 Confocal Light microscopy
614 Three imaging setups have been used for fixed samples-
615 1. Olympus FV1000 laser scanning confocal microscope on Olympus BX61 inverted stand and driven by
616 FV10-ASW 1.7 software. Brain and ring gland whole mounts were imaged with Olympus UApochromat 40x
617 1.3NA oil immersion objective. Corpora cardiaca cells were imaged with Olympus UApochromat 60x 1.35
618 NA oil immersion objective.

619 2. Andor spinning disc confocal microscope on Olympus IX81 inverted stand using Andor iXON 897 EMCCD
620 camera with Yokogawa CSUX1 scanhead, running on Andor software. Some fat bodies were imaged with
621 Olympus U Plan SApo 60x/ 1.35NA oil immersion objective.
622 3. Olympus FV3000 laser scanning confocal microscope on Olympus IX83 inverted stand and driven by
623 FV31S-SW acquisition software. Corpora cardiaca cells and wing discs were imaged with Olympus
624 UPLXApochromat 60x 1.42 NA oil immersion objective.
625
626 Electron microscopy
627 **Morphology:** Dissected brain-ring gland complexes were initially fixed in PBS with 2%PFA (cat#16005,
628 Aldrich) and 1% glutaraldehyde (cat#G5882, Sigma) for 2 hours at room temperature followed by overnight
629 incubation at 4˚C. Then the samples were post-fixed with 1% OsO4 (cat# 19190, EMS) and 1.5% potassium
630 ferrocyanide (cat#: P9387, Sigma-Aldrich) in water on ice for 1 hour. En bloc staining was done in the dark
631 with 1% UA (cat# 21447, Polyscience Europe GmbH) in water at 4˚C overnight. Following infiltration and
632 embedding, 70nm sections were cut on a Leica Ultracut UCT (Leica Microscopy systems) and picked up with
633 formvar (cat# 15800, EMS) coated slot grids (cat# G2010-Cu, EMS). All samples were then post-stained with
634 1% UA (cat# 21447, Polysciences Europe GmbH) in water for 10 minutes and 0.04% lead citrate (cat# 17800,
635 EMS) for 5 minutes. Electron micrographs were obtained at 80kV using Morgagni (Emsis Morada CCD
636 camera, formerly Sys/Olympus) and 100kV using Tecnai 12 (TVIPS F416 camera) electron microscopes (both
637 from Thermo Fisher Scientific (formerly FEI/Philips)).
638
639 **Immunogold labelling:** Dissected brain-ring gland complexes were initially fixed in PBS with 4% PFA and
640 0.05% glutaraldehyde for 20 minutes at room temperature. Post-fixation was done in 1:1 dilution of the
641 initial fixative overnight at 4˚C. Ring glands were then embedded with 12% gelatin (cat# G-2500, Sigma-
642 Aldrich) in PBS and infiltrated with 2.3M sucrose (cat# 21600, EMS) in PBS overnight at 4˚C. The sucrose
643 infiltrated Ring gland in gelatin was mounted on an aluminum pin and snap frozen in LN2 and cryosectioned
644 on a Leica Ultracut EM UC6 ultramicrotome (Leica Microscopy systems). 70nm Sections were picked up
645 using a 1 :1 mixture of 2.3M sucrose and 2% methyl cellulose (cat# M-6385, Sigma-Aldrich) as a pick-up
646 solution and sections were transferred to carbon and formvar coated mesh grids (cat# H100-Cu, EMS). After
647 removal of gelatin by incubation on PBS at 37 ˚C, sections were labelled with rabbit-anti-Dilp2/Dilp5 or goat-
648 anti-AKH Antibody (diluted 1 to 20 or 1 to 100 from original antibody solution) followed by secondary
649 antibody coupled to 10-nm gold (British Biocell or Bbisolutions) and secondary fluorescence antibodies
650 (donkey-anti-rat Alexa594 cat# A-21209, Molecular Probes Europe B.V., goat-anti-rabbit Alexa488 cat# A-
651 21206, Mol. Probes Europe B.V.) The sections were first imaged with epifluorescence on a Zeiss upright

652 ApoTome microscope with Axiocam506 camera to locate regions of interest in individual sections and
653 contrasted with a mixture of 1.9% methyl cellulose/0.3% UA for 10min on ice and the corresponding regions
654 of interest were observed by using a Morgagni or Tecnai12 electron microscope.
655
656 **Image analysis and quantification**
657 **Whole cell:** Individual cells from multiple samples were manually segmented and mean intensity was
658 measured using Fiji/ImageJ (Schindelin et al., 2012) .
659 **Co-localization :** Single confocal images from two different channels were used in Coloc 2 plugin in
660 Fiji/ImageJ (Schindelin et al.,2012) .
661 **Nuclear and cytoplasmic intensity ratio:** Regions of interested were manually drawn on respective tissues.
662 Nuclear to cytoplasmic intensity ratio was then calculated using a Fiji/ImageJ macro developed by Volker
663 Baecker at Montpellier RIO Imaging (Intensity Ratio Nuclei Cytoplasm Tool, RRID:SCR_018673).
664 Documentation can be accessed here . Same analysis parameters were used across samples compared.
665 **Electron micrographs:** For morphological sections, composite images were assembled in Fiji (Schindelin et
666 al., 2012) using ImageJ TrackEM2 plugin (Cardona et al., 2012). For immunogold labelling, regions of interest
667 were visually determined and gold particles were hand-counted in Fiji/ImageJ.
668 **Wing area:** Each wing blade was hand segmented and area measured in pixels using a self-written macro
669 on Fiji/ImageJ.
670 **Pupal volume:** Using a self-written Fiji/Imagej macro, an ellipse was fitted to the pupa. Volume was
671 calculated assuming an ellipsoid using the formula below (minor axis length as the height) -
672 $$\text{Volume} = 0.75\pi * (\text{major-axis}) * (\text{minor-axis})^2.$$
673
674 **Data representation and statistical analysis**
675 Data wrangling was done using Microsoft Excel and R-Studio (version 1.3.1093). R-Studio was also used for
676 plotting. Packages used in R- plyr, dplyr, ggplot2 and xlsx. Plots generated through R were then formatted
677 using Adobe Illustrator 2021. Illustrations were generated using BioRender (www.biorender.com).
678 Statistical analysis was done using Microsoft Excel, GraphPad Prism 5.0 and online through
679 https://www.socscistatistics.com . Information about sample sizes and statistical tests used in this study can
680 be found in the respective figure legends. Detailed information on sample size and replicates have also been
681 summarized in **Table 1** of the supplementary material.
682

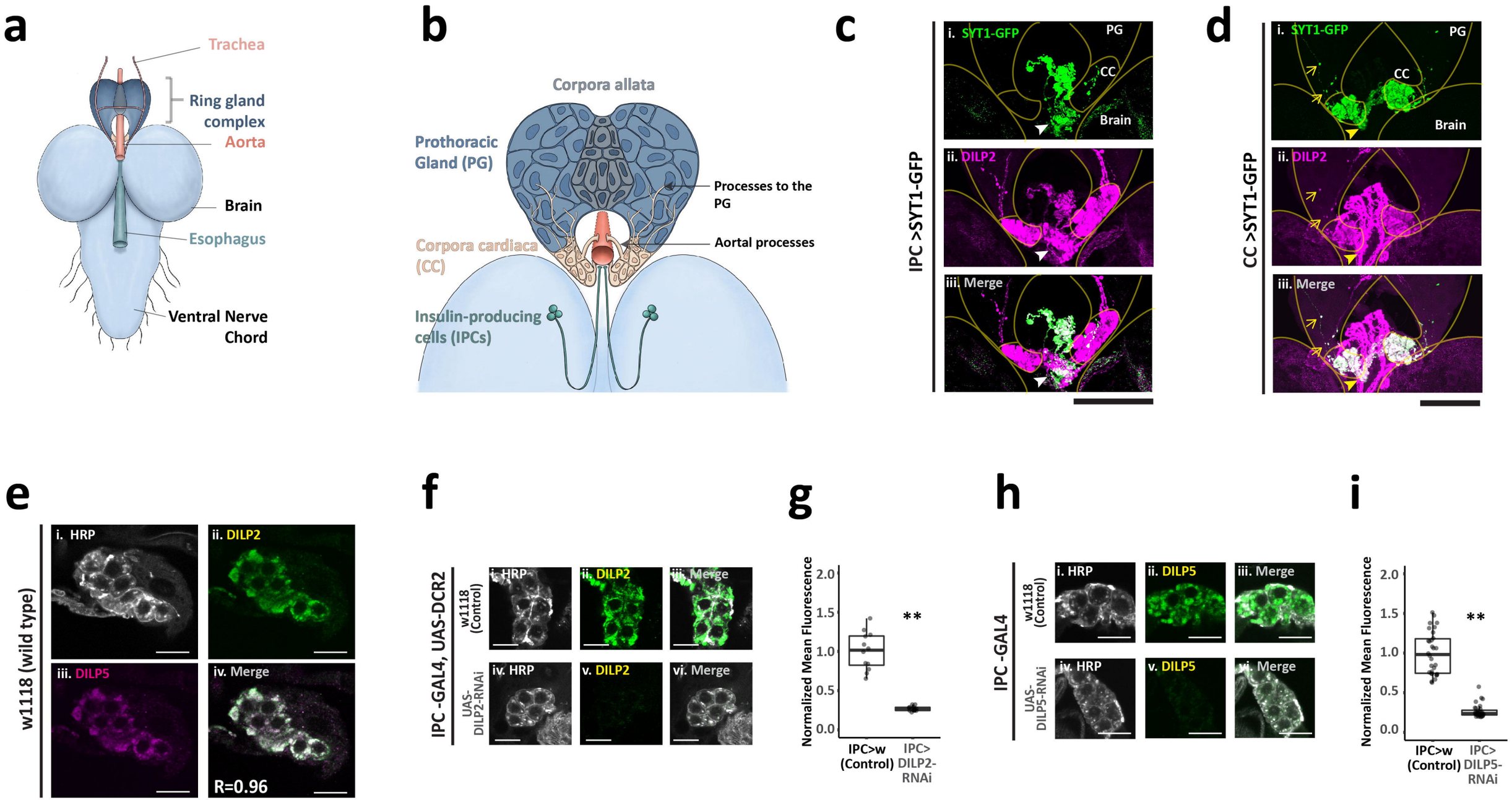
a
Trachea
Ring gland complex
Aorta
Brain
Esophagus
Ventral Nerve Chord
b
Corpora allata
Prothoracic Gland (PG)
Processes to the PG
Aortal processes
Corpora cardiaca (CC)
Insulin-producing cells (IPCs)
c
IPC >SYT1-GFP
i. SYT1-GFP
PG
CC
Brain
ii. DILP2
iii. Merge
d
CC >SYT1-GFP
i. SYT1-GFP
PG
CC
Brain
ii. DILP2
iii. Merge
e
w1118 (wild type)
i. HRP
ii. DILP2
iii. DILP5
iv. Merge
R=0.96
f
IPC -GAL4, UAS-DCR2
w1118 (Control)
UAS-DILP2-RNAi
i. HRP
ii. DILP2
iii. Merge
iv. HRP
v. DILP2
vi. Merge
g
Normalized Mean Fluorescence
2.0
1.5
1.0
0.5
0.0
**
IPC>w (Control)
IPC> DILP2-RNAi
h
IPC -GAL4
w1118 (Control)
UAS-DILP5-RNAi
i. HRP
ii. DILP5
iii. Merge
iv. HRP
v. DILP5
vi. Merge
i
Normalized Mean Fluorescence
2.0
1.5
1.0
0.5
0.0
**
IPC>w (Control)
IPC> DILP5-RNAi

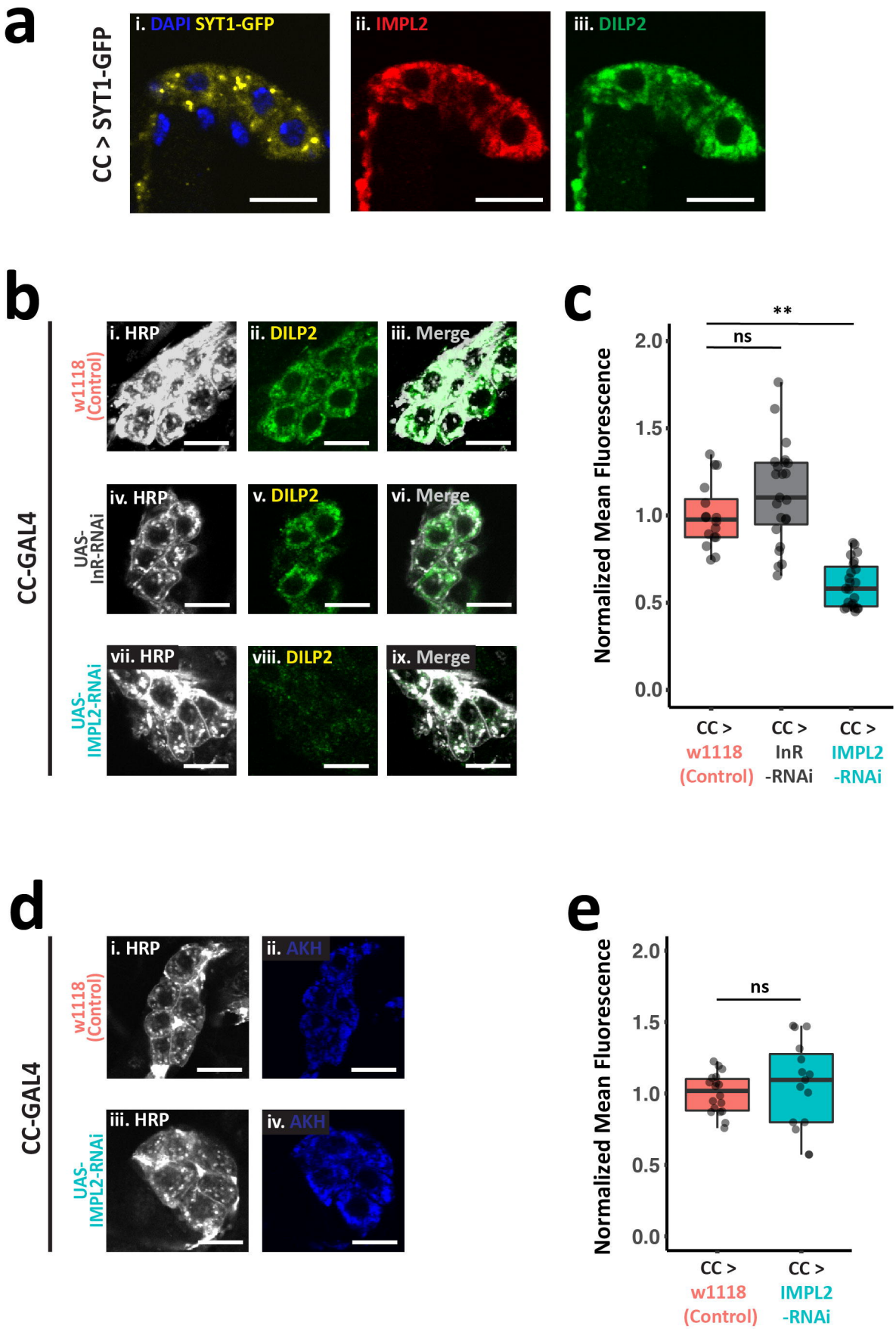
a
CC > SYT1-GFP
i. DAPI SYT1-GFP
ii. IMPL2
iii. DILP2
b
CC-GAL4
w1118 (Control)
UAS-InR-RNAi
UAS-IMPL2-RNAi
i. HRP
ii. DILP2
iii. Merge
iv. HRP
v. DILP2
vi. Merge
vii. HRP
viii. DILP2
ix. Merge
c
Normalized Mean Fluorescence
2.0
1.5
1.0
0.5
0.0
ns
**
CC > w1118 (Control)
CC > InR -RNAi
CC > IMPL2 -RNAi
d
CC-GAL4
w1118 (Control)
UAS-IMPL2-RNAi
i. HRP
ii. AKH
iii. HRP
iv. AKH
e
Normalized Mean Fluorescence
2.0
1.5
1.0
0.5
0.0
ns
CC > w1118 (Control)
CC > IMPL2 -RNAi

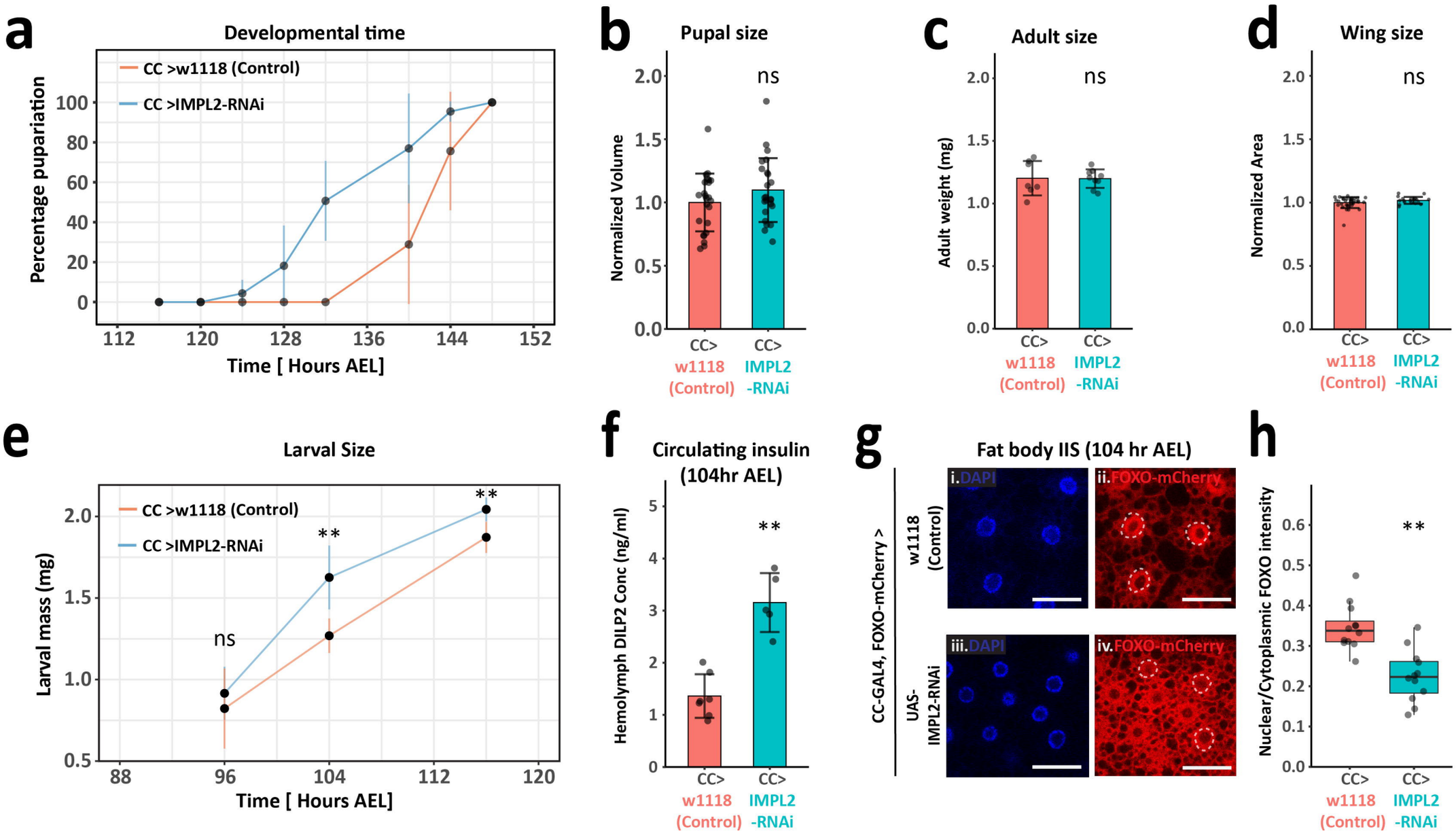
a
Developmental time
CC >w1118 (Control)
CC >IMPL2-RNAi
Percentage pupariation
Time [Hours AEL]
b
Pupal size
ns
Normalized Volume
CC> w1118 (Control)
CC> IMPL2 -RNAi
c
Adult size
ns
Adult weight (mg)
d
Wing size
ns
Normalized Area
e
Larval Size
CC >w1118 (Control)
CC >IMPL2-RNAi
ns
**
**
Larval mass (mg)
Time [Hours AEL]
f
Circulating insulin (104hr AEL)
**
Hemolymph DILP2 Conc (ng/ml)
g
Fat body IIS (104 hr AEL)
CC-GAL4, FOXO-mCherry >
w1118 (Control)
UAS-IMPL2-RNAi
i.DAPI
ii.FOXO-mCherry
iii.DAPI
iv.FOXO-mCherry
h
**
Nuclear/Cytoplasmic FOXO intensity

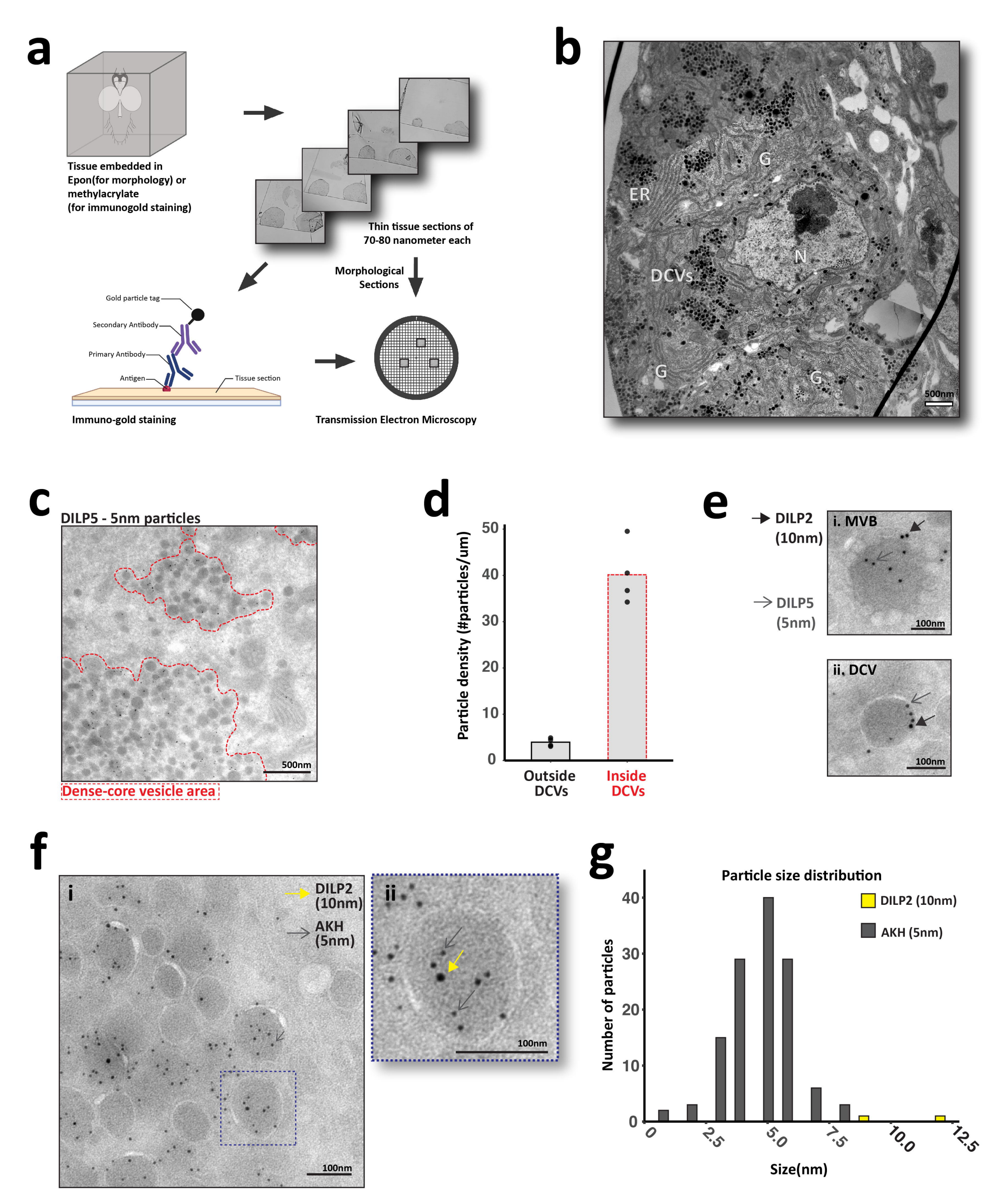
a
Tissue embedded in Epon(for morphology) or methylacrylate (for immunogold staining)
Thin tissue sections of 70-80 nanometer each
Morphological Sections
Gold particle tag
Secondary Antibody
Primary Antibody
Antigen
Tissue section
Immuno-gold staining
Transmission Electron Microscopy
b
G
ER
N
DCVs
G
G
500nm
c
DILP5 - 5nm particles
500nm
Dense-core vesicle area
d
Particle density (#particles/um)
50
40
30
20
10
0
Outside DCVs
Inside DCVs
e
DILP2 (10nm)
DILP5 (5nm)
i. MVB
100nm
ii. DCV
100nm
f
i
DILP2 (10nm)
AKH (5nm)
100nm
ii
100nm
g
Particle size distribution
DILP2 (10nm)
AKH (5nm)
Number of particles
40
30
20
10
0
0
2.5
5.0
7.5
10.0
12.5
Size(nm)

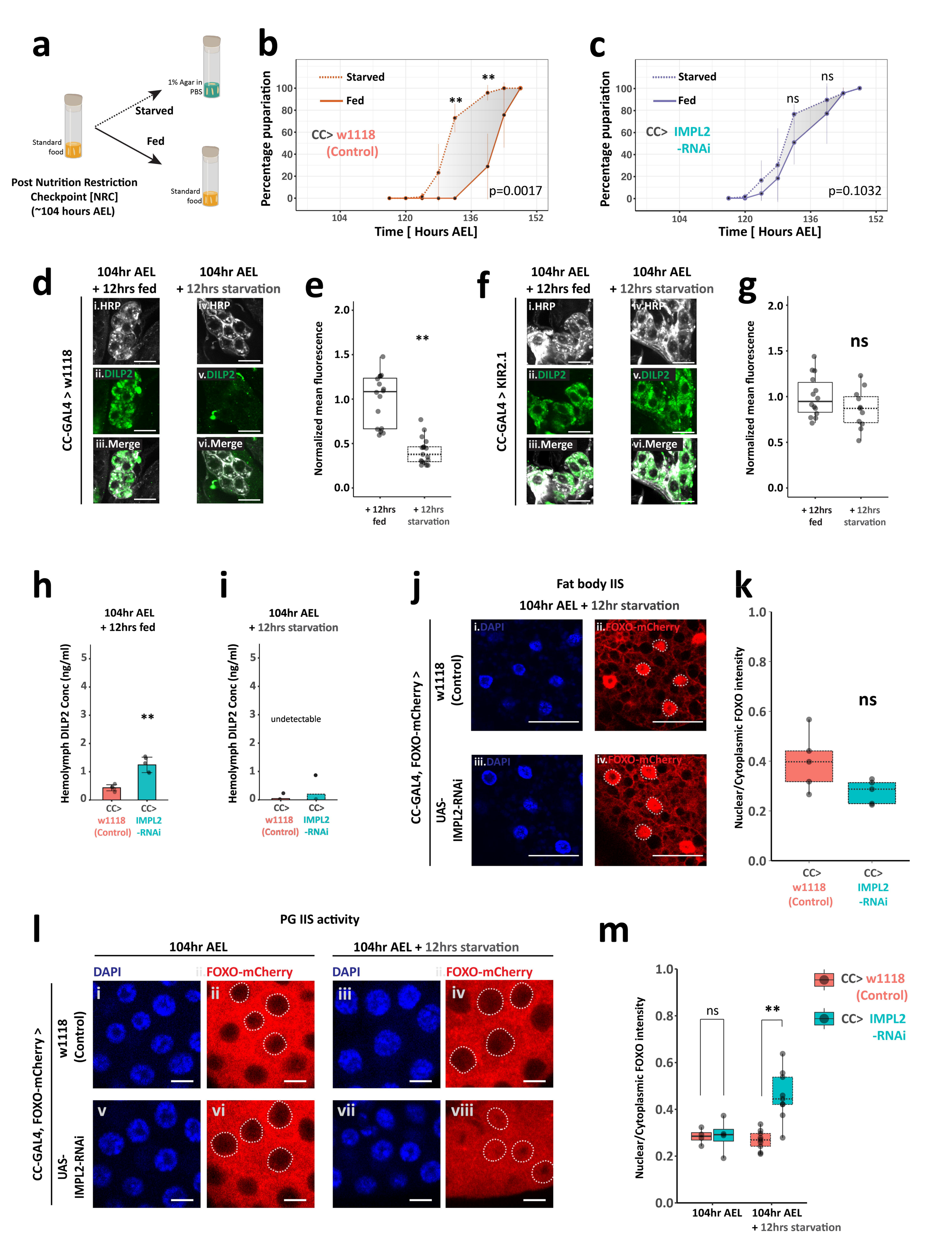
a
1% Agar in PBS
Starved
Fed
Standard food
Standard food
Post Nutrition Restriction Checkpoint [NRC] (~104 hours AEL)
b
Starved
Fed
CC> w1118 (Control)
Percentage pupariation
Time [Hours AEL]
p=0.0017
c
Starved
Fed
CC> IMPL2 -RNAi
Percentage pupariation
Time [Hours AEL]
p=0.1032
d
104hr AEL + 12hrs fed
104hr AEL + 12hrs starvation
CC-GAL4 > w1118
i.HRP
ii.DILP2
iii.Merge
iv.HRP
v.DILP2
vi.Merge
e
Normalized mean fluorescence
+ 12hrs fed
+ 12hrs starvation
f
104hr AEL + 12hrs fed
104hr AEL + 12hrs starvation
CC-GAL4 > KIR2.1
i.HRP
ii.DILP2
iii.Merge
iv.HRP
v.DILP2
vi.Merge
g
Normalized mean fluorescence
+ 12hrs fed
+ 12hrs starvation
h
104hr AEL + 12hrs fed
Hemolymph DILP2 Conc (ng/ml)
CC> w1118 (Control)
CC> IMPL2 -RNAi
i
104hr AEL + 12hrs starvation
Hemolymph DILP2 Conc (ng/ml)
undetectable
CC> w1118 (Control)
CC> IMPL2 -RNAi
j
Fat body IIS
104hr AEL + 12hr starvation
CC-GAL4, FOXO-mCherry >
w1118 (Control)
UAS-IMPL2-RNAi
i.DAPI
ii.FOXO-mCherry
iii.DAPI
iv.FOXO-mCherry
k
Nuclear/Cytoplasmic FOXO intensity
CC> w1118 (Control)
CC> IMPL2 -RNAi
l
PG IIS activity
104hr AEL
104hr AEL + 12hrs starvation
DAPI
FOXO-mCherry
CC-GAL4, FOXO-mCherry >
w1118 (Control)
UAS-IMPL2-RNAi
m
Nuclear/Cytoplasmic FOXO intensity
CC> w1118 (Control)
CC> IMPL2 -RNAi
104hr AEL
104hr AEL + 12hrs starvation